Spin flip transitions in ^{13}C and ^{19}F probed with the (π^-,γ) reaction

C. J. Martoff,* J. A. Bistirlich, C. W. Clawson, K. M. Crowe, M. Koike,†
J. P. Miller,‡ S. S. Rosenblum, and W. A. Zajc
Lawrence Berkeley Laboratory, University of California, Berkeley, California 94720

H. W. Baer and A. H. Wapstra§
Los Alamos Scientific Laboratory, Los Alamos, New Mexico 87545

G. Strassner** and P. Truöl
Physik-Institut der Universität Zürich, Ch 8001 Zurich, Switzerland
(Received 6 December 1982)

Photon spectra from radiative capture of stopped negative pions captured by ^{13}C and ^{19}F nuclei have been measured with a high resolution pair spectrometer. In the bound region transitions have been observed to ^{13}B(g.s.), ^{13}B(3.5 MeV), ^{19}O(g.s.), ^{19}O(4.9 MeV), and ^{19}O(6.3 MeV). In addition, strong transitions to narrow states above the neutron separation threshold were observed in both cases. The results for ^{13}C are in agreement with detailed shell model calculations of this process. Major strength is observed for states formed by coupling extra nucleons or holes to the spin-quadrupole $d_{5/2}$ and $d_{3/2}$, $J^\pi=2^-$ states in ^{16}O. The $^{13}C(\pi^-,\gamma)^{13}B_{g.s.}$ branching ratio is shown to be consistent with beta decay and electroexcitation data, through a combined phenomenological analysis. The observed transition strengths are accounted for by matrix elements of the spin-density operators $[\sigma\times Y_0]^1t^+$ and $[\sigma\times Y_1]^2t^+$.

[NUCLEAR REACTIONS $^{13}C(\pi^-,\gamma)$, $^{19}F(\pi^-,\gamma)$; measured normalized $I(E_\gamma)$; deduced upper limit on $\delta(E2/M1)$ for $^{13}C\rightarrow{}^{13}B$(g.s.) at $q=125$ MeV/c, systematics of SIGDR in $12\leq A\leq 20$. Stopped π^-; pair spectrometer; 850 keV at 129.4 MeV.]

I. INTRODUCTION

Within the $1p$ and $2s$-$1d$ shell, radiative pion capture spectra have been successfully analyzed to extract information on strong magnetic transitions with large spin density matrix elements.[1-3] Such transitions are of $M1$ to $M3$ type, and have been observed for nuclides from ^{10}B to ^{28}Si. The sensitivity to such transitions arises from the nature of the (π^-,γ) transition operator. As long as pion absorption is restricted to the lower pionic orbits, the operator is dominated by Gamow-Teller ($[\sigma\times Y_0]^1t^+$) and spin-dipole ($[\sigma\times Y_1]^2t^+$) pieces, and therefore connects states with strong matrix elements of these operators. This peculiarity of the (π^-,γ) reaction is experimentally well established and supported by detailed shell model calculations.

The most studied examples are the nuclides ^{12}C (Ref. 4) and ^{16}O (Refs. 5 and 6), where prominent $M2$ (spin-dipole) excitations ($\Delta J^\pi=2^-$) dominate the spectra. ^{18}O data[6] have further shown that adding two neutrons produces a core polarization,[7] evidenced by a shift of 3.4 MeV in the spectrum, but otherwise no drastic change. However, in ^{14}N the magnetic quadrupole resonances are less pronounced,[8,9] showing that the coupling of the extra proton to the excitations of the core smears the strength considerably. The purpose of the present experimental investigation was to select two further cases near the end of the $1p$ shell or the beginning of the $2s$-$1d$ shell to test these findings.

For ^{13}C the extra neutron is expected[10] to couple only weakly to the dominant ^{12}C transitions, and to produce only a narrow splitting of the 2^- levels into $\frac{5}{2}^+$ and $\frac{3}{2}^+$ doublets. For ^{19}F we expect similar behavior, although no detailed calculations are available. These expectations are indeed supported by our data, which provides in both cases the first clues to the structure of the high-lying $\Delta T=1$ isovector states in $A=13$ and 19.

A second goal of our experiment was to investigate quantitatively the $^{13}C\rightarrow{}^{13}B$(g.s.) giant $M1$ transition. Here a phenomenological analysis can be applied which links the (π^-,γ) branching ratio to beta

decay, inelastic electron scattering, and gamma decay through the different isospin components of the $[\sigma \times Y_0]^1 t^i$ operator. This technique has previously been used [e.g., in ^{20}Ne (Ref. 11)], to explore a large contribution from the orbital magnetization to an $M1$ transition. For ^{13}C we extend the technique for the first time to spin-flip-$E2$ matrix elements.

This article is organized as follows. In Sec. II, a brief account of the experimental apparatus and method is given. Section III is devoted to the phenomenological analysis of the bound state transition. In Sec. IV we discuss the high excitation region for $^{13}C(\pi^-,\gamma)$ and $^{19}F(\pi^-,\gamma)$. The ^{13}C data are compared with shell model calculations of the Dubna group.[10] The magnetic quadrupole transitions and their trend from $A=13$ to 20 are discussed. In Sec. V we conclude with a short summary.

II. EXPERIMENTAL ASPECTS

A. Apparatus

The experiments were performed at the Low Energy Pion Channel of the Clinton P. Anderson Meson Physics Facility (LAMPF), Los Alamos Scientific Laboratory. A scheme of the experimental apparatus is shown in Fig. 1. The beam of up to 6 times 10^6 π^- per second was stopped in the targets to be studied by passing it through a polyethylene degrader stack. The degrader thickness was optimized for each target by measuring the fraction of pions stopping in the target with a three element beam telescope, at reduced beam fluxes. A liquid hydrogen target was used for efficiency, line shape, and calibration measurements, which were interspersed with the data runs.

During data taking, the incident pion flux was monitored by a two element telescope, not pictured, which counted particles backscattered from the upstream side of the degrader stack. This monitor was calibrated against the three element beam telescope at reduced beam flux.

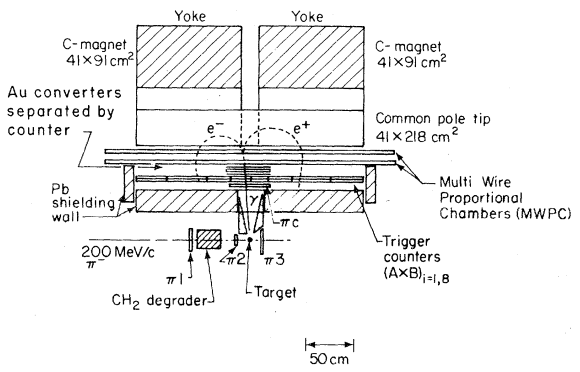

FIG. 1. Schematic of the experimental apparatus.

The pair spectrometer consisted of a twin-C magnet with common pole tip,[5] two large multiwire proportional chambers (MWPC), a set of trigger counters, the photon converter foils, and the associated electronics. Briefly stated, the spectrometer worked as follows. Photons from the target passed through the collimating aperture, and through a thin plastic scintillator which was used to discriminate against charged particles. After further passing through a pair of trigger counters, a small fraction of the photons were converted into e^+e^- pairs in the gold converter foils. The pairs were separated and bent through about 180 deg in the magnetic field. Upon entry and exit from the field region, the pairs passed through the MWPC's, where their coordinates were measured. Upon exit from the magnetic field region, the electron and positron passed through two nonadjacent trigger counters. This signature combined with fast MWPC signals and the absence of a charged particle veto pulse defined an "event." In this case the triggering electronics were gated off, the MWPC information encoded and read out, and all the data collected in a computer memory buffer destined to be written on tape when filled.

A more detailed description of the parts of the spectrometer will now be given. The magnet provided a nominal field of 0.8 T over a rectangular volume 33 cm high, 218 cm long, and 41 cm deep. The LAMPF technical staff measured the three spatial components of the field on a 2.54 cm^3 grid throughout this volume to an accuracy of 10^{-4} T. The complete map was used in the analysis procedure described in Sec. II B. The magnet excitation was monitored by a water cooled shunt and a Hall probe, and was constant to within $\pm 0.25\%$ during the data taking discussed here. The field volume was filled by a helium bag with 25 μ Mylar walls to reduce multiple scattering of the e^+e^- pairs.

Two MWPC's were suspended between the target and the magnet. The chambers and their readout system were designed and built at Lawrence Berkeley Laboratory (LBL).[12] Each chamber had an active area of 25×200 cm, with three signal planes. These wires ran vertically and at ± 30 deg from the vertical, with 0.2 cm between wires. This arrangement identifies even rather closely spaced crossing points without ambiguity, and has nearly equal spatial resolution in the horizontal and vertical directions. The "magic" gas was used (argon, isobutane, methylal, Freon). The chambers were shielded from beam and room background by a 20 cm thick lead wall, with a collimating aperture viewing the pion capture target. The aperture was completely covered by a 0.3 cm thick plastic scintillator ($\pi - C$)

which was used to veto possible event triggers from the copious flux of scattered charged particles entering the aperture.

Two converter foils were used, a "thick" 0.01 cm×7 cm×20 cm gold foil, followed by a 0.3 cm thick plastic scintillator and another, "thin" 0.005 cm×6.5 cm×19 cm gold foil. Photons converting in the thick foil were distinguished by the presence of a pulse in the scintillator. This arrangement allowed the simultaneous acquisition of two data samples. The events from the thin converter have very good energy resolution, and the thick converter events have more modest resolution but are twice as numerous. This arrangement was required for an in-flight capture test experiment, performed later in the data-taking period. Only thin converter data are presented here, because of their superior energy resolution.

Eight pairs of 4 mm thick trigger counters were mounted across the target side of the MWPC's. Counter pairs 1,2,7,8 were 30 cm×30 cm and pairs 3,4,5,6 were 15 cm×30 cm. Any coincidences $(AI\times BI)\times(AJ\times BJ)$ with $2<|I-J|<7$ defined a "gamma" (γ). An event trigger was defined by $(\gamma)\times(\overline{\pi-C})\times(>3$ planes of MWPC firing$)\times(\pi$ stop). The beam telescope signature "π stop" was included only during reduced rate measurements for normalization.

The branching ratios were obtained by comparison with the precisely known π^-+proton $\rightarrow$neutron$+\gamma$ branching ratio of 0.393 $\pm$0.001 (Ref. 13). The fraction of pions stopping in the target was measured with the beam telescope. The dependence of the acceptance upon energy (relative to the hydrogen line) was obtained by comparing the ^{12}C spectrum measured in the present experiment to previous work[4] and from the shape of the π^-+ proton$\rightarrow$neutron$+\pi^0$ continuum.

The ^{13}C target used was 0.53 g/cm^2 of 99% isotopically pure graphite powder.[14] The powder was packed into pouches made of ^{12}C-containing Mylar. A 15% background from the pouches was measured with identical empty pouches and subtracted from the data later.

Two fluorine-containing targets were used, LiF and Teflon (CF_2). The ^{19}F spectrum was found from a fit to the LiF and CF_2 spectra[15] using the known $^7Li(^6Li)$ and ^{12}C spectra.[9] The capture probability on ^{19}F was found to be 89.4$\pm$0.7 % for CF_2 and 82.2$\pm$1.4 % for LiF.

B. Data analysis

After the experiment, a computer program scanned the MWPC information on tape for patterns of crossing points characteristic of an e^+e^- pair. Twenty-two percent of the event triggers were accepted by this scan.

Multiparametric polynomial fits to the entrance angles and momenta as functions of the MWPC crossing points were obtained from computer simulated events.[16,17] This method is very economical of computer time, eliminating the need to iteratively fit each data event to be analyzed. The particle vector momentum is obtained from an analytic formula, with accuracy at least as good as obtained by iterative fitting, and using less than one fourth the computing time.

Using the angles so obtained, the pairs were extrapolated back to the converter foils and the pion capture targets. Cuts were applied to the separation of the e^+ and e^- at the converter foil, and to the origin in the target plane. These cuts eliminated photons not coming from the target, those which converted before the gold foils and yet were not vetoed by $\pi-C$, and electrons which suffered unusually large multiple scatterings in the converter. The FWHM energy resolution (for the thick converter data) and the "tails" of the line shape (for both thick and thin converters) were significantly improved by the cuts. The cuts removed 10% of the thin converter events and 30% of the thick converter events, resulting in final FWHM energy resolutions of 850 and 1750 keV, respectively, for the monochromatic photons of π^-+ proton$\rightarrow$neutron$+\gamma$ (129.4 MeV), as evidenced by the upper line in the ^{13}C spectrum (Fig. 2).

C. Results

In Figs. 2 and 3 we present the experimental spectra and the fits which gave the partial and total branching ratios summarized in Tables I and II. Partial branching ratios to individual final states were obtained by fitting the spectrum to a sum of sharp lines (for bound or slightly unbound levels) and a smooth background[1,18] due to the radiative capture into the breakup channel. The individual contributions were folded with the measured line shape and include the acceptance correction.

In order of decreasing photon energy the peaks in Fig. 2 can be associated with: the ^{13}B ground state ($E_\gamma=125.0$ MeV), an unresolved doublet of a $\frac{3}{2}^+$ and a $\frac{5}{2}^+$ state near 3.5 MeV excitation ($E_\gamma=121.5$ MeV), another doublet of sharp states at 6.5 and 7.6 MeV excitation (these lie above the breakup threshold of 4.9 MeV), and a broad level or group of overlapping levels near 10.2 MeV. We will return to a detailed discussion of these levels in Sec. III. At this point we only stress the close correspondence of these experimental results with the ^{12}C case, as shown by Fig. 4. In ^{12}C, transition to the ^{12}B

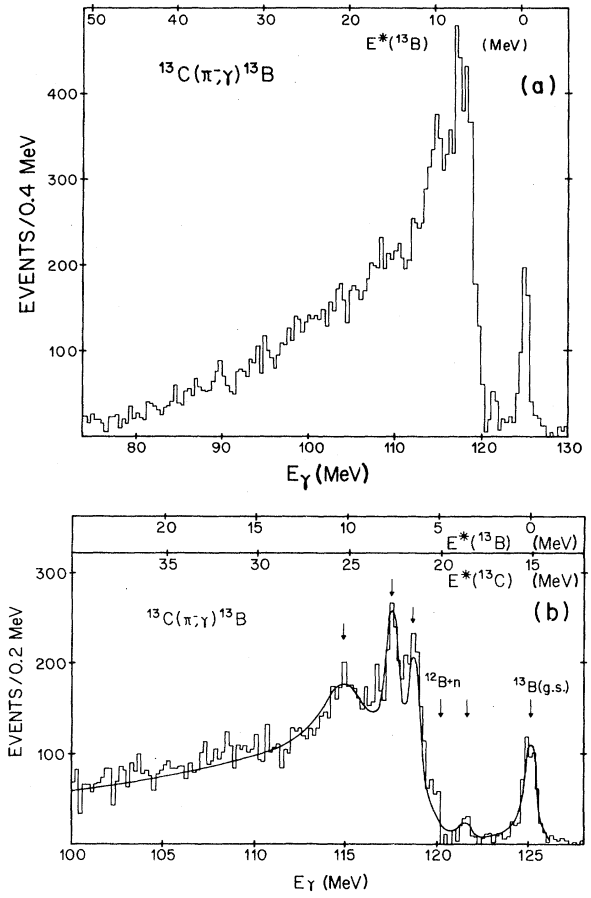

FIG. 2. (a) Photon spectrum for $^{13}C(\pi^-,\gamma)$ obtained in the present work. The fitted curve giving the experimental branching ratios is shown superimposed in (b).

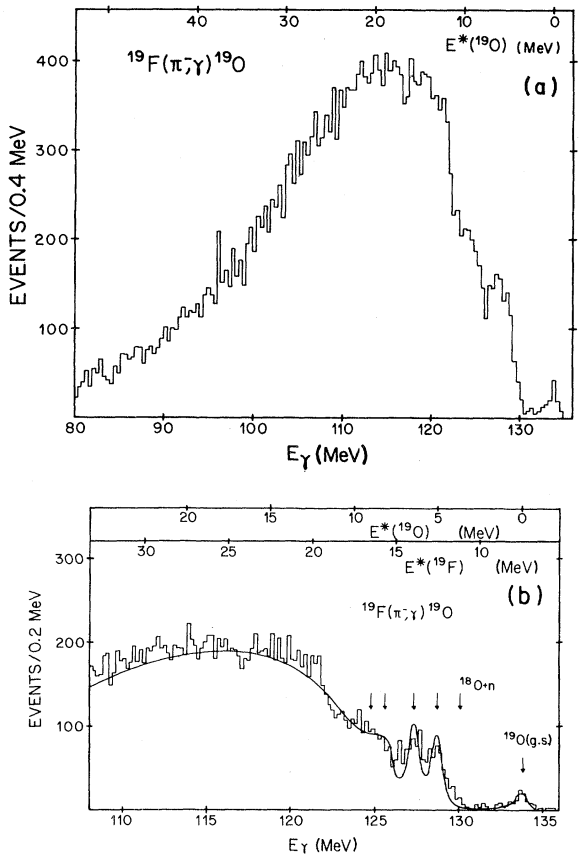

FIG. 3. (a) Photon spectrum for $^{19}F(\pi^-,\gamma)$ obtained in the present work. (b) The fitted curve giving the experimental branching ratios is shown superimposed on (a).

$J^\pi = 1^+$ ground state was observed with a branching ratio of $(6.2\pm0.4)\times10^{-4}$. At 1.67 and 2.62 MeV in ^{12}B, a 2^- and a 1^- state were found with branching ratios of $(0.5\pm0.2)\times10^{-4}$ and $(1.1\pm0.2)\times10^{-4}$, respectively.[4,9] The sum of the branching ratios to the 6.5 and 7.6 MeV doublet in ^{13}C $(18.8\pm2.8)\times10^{-4}$, compares favorably with the $(18.3\pm0.6)\times10^{-4}$ seen in ^{12}B for the largest peak at 4.5 MeV excitation.[9] This state was the original spin-isospin excitation discovered with the (π^-,γ) reaction. In both cases the quasifree background is well fitted by the pole-model ansatz,[1,18] which is mainly used to obtain the total branching ratio. The recoiling ^{12}B is taken to be in its ground state here. The total branching ratios for ^{12}C and ^{13}C are also quite similar, being $1.84\pm0.08\times10^{-2}$ (Ref. 9) and $1.92\pm0.19\times10^{-2}$ (Ref. 4) for ^{12}C, and $1.66\pm0.25\times10^{-2}$ for ^{13}C (present work). In Table I

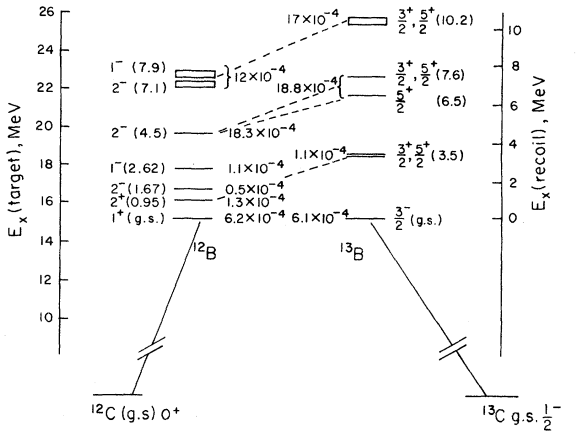

FIG. 4. Levels in boron isotopes excited by (π^-,γ) on carbon isotopes. The patterns in ^{12}B and ^{13}B are very similar, aside from minor shifts of the core-excited states and splitting due to the extra neutron in ^{13}B. Radiative capture branching ratios from Ref. 9 (^{12}C) and the present work (^{13}C) are given, as well as the excitation energy and spin parity for the states.

TABLE I. Experimental branching ratios and levels in ^{13}C, and predictions of Ref. 10.

	E_γ (MeV)					Pole	
	125.0	121.5	118.5	117.4	114.8	120.1[g]	Total
$E_x(^{13}C)$[a] (MeV)	15.1	18.6	21.6	22.7	25.3	20.0[g]	
$E_x(^{13}B)$ (MeV)	0.0	3.5	6.5	7.6	10.2	4.9[g]	
$R(10^{-4})$[b] (MeV)	6.1±1.0	1.0±0.5	8.3±1.5	9.0±1.6	17.4±3.6	122.7±18.8	166±25
$R/R_{tot}(10^{-2})$	3.7	0.6	5.1	5.5	10.5	74.6	100
N_{fit}[c]	704±50	112±51	967±97	1039±205	2007±286	14200±359	19030±486
Γ_γ (MeV)					2.1±0.5		
$E_x(^{13}B)$[d] (MeV)	0.0	3.53/3.68	6.42	7.52/7.86			
$E_x(^{13}C)$[d] (MeV)	15.11	18.75	21.81		25.5		
$E_x(^{13}B)$[e] (MeV)	0.0	3.5/3.9	5.5	6.4	8.0–11.6		
R[f](10^{-4})	12.8	7.9	11.4	24.1	37.9		
$J^\pi, T=\frac{3}{2}$	$\frac{3}{2}^-$	$\frac{3}{2}^\pm, \frac{5}{2}^{+h}$	$\frac{3}{2}^{+h}$	$\frac{5}{2}^{+h}$	$\frac{3}{2}^+, \frac{5}{2}^{+h}$		

[a]Excitation energy of analog levels in ^{13}C.
[b]Includes normalization uncertainty.
[c]Number of events from fit to spectrum.
[d]From other experiments; see Tables 13.1 and 13.4 of F. Ajzenberg-Selove, Nucl. Phys. A268, 1 (1976).
[e]Theoretical energies, Ref. 10.
[f]Predicted branching ratio, Ref. 10.
[g]End point energy, $\Delta=18.8$ MeV; see Ref. 1.
[h]Quantum number assignments from shell model calculations, Ref. 10.

the information available on these levels from other reactions is also summarized.

In ^{19}F the fit is much less unambiguous. Only the unresolved doublet ^{19}O(g.s.), ^{19}O(0.1 MeV) at 133.6 MeV, and two levels at 4.9 and 6.3 MeV excitation (128.6 and 127.2 MeV photon energy) can be clearly identified. The breakup threshold is at 4.6 MeV excitation. Even for the two latter levels, the fit is not too good. The high excitation energy region is reasonably well fitted by the pole-model ansatz if the excitation energy of the ^{18}O recoil is taken to be 5.0 MeV, close to the first $J^\pi=2^-$ level in ^{18}O (5.5 MeV). This finding is quite similar to ^{16}O and ^{18}O, where the recoiling nuclides are not in their ground states.[6] The two levels found near 8.0 and 8.8 MeV are not well established in position or strength. The difficulties in representing the continuum preclude firmer conclusions. For the same reason we have not attempted to associate a branching ratio with the step in the spectrum seen near 120 MeV photon en-

TABLE II. Experimental branching ratios $^{19}F(\pi^-,\gamma)^{19}O$.

E_γ	E_x ^{19}F (MeV)	E_x ^{19}O (MeV)	R_γ[b] (10^{-4})	N_{fit}[c]	R/R^{total} (10^{-2})
133.6	7.5[d]	0.0	1.3 ±0.3	166 ±20	0.6
128.6	12.5	4.9	4.5 ±1.2	562 ±90	1.9
127.2	13.9	6.3	4.8 ±1.2	584 ±118	2.0
125.6	15.5	8.0	3.2 ±0.8	401 ±50	1.4
124.8	16.3	8.8	2.7 ±0.6	333 ±23	1.1
$\Gamma=0.34$ MeV (124.1)[a]	(16.5)[a]	(9.0)[a]	223 ±46	27 300 ±375	93.0
		Total	240 ±48	29 350 ±381	100.0

[a]End point energy of fitted pole model ($\Delta=14.3$ MeV, see Ref. 1).
[b]Radiative branching ratio, including normalization error.
[c]Number of events found in fit to spectrum.
[d]M. Wiescher *et al.*, Nucl. Phys. A349, 165 (1980), Fig. 22.

ergy. We will, however, deal with this structure qualitatively in Sec. III.

III. THE $^{13}C(\pi^-,\gamma)^{13}B$(g.s.) TRANSITION: PHENOMENOLOGICAL ANALYSIS

A. Theoretical background of the phenomenological analysis

For $J=0$ targets in the 1-p shell, the well-known strong $M1$ transitions and their β decay analogs have long been compared in order to separate the spin and orbital parts of the $M1$ operator.[19,20] When no β decay is available, use of the (π^-,γ) branching ratio has been shown to allow this separation as well.[2,7,11] The radiative pion capture reaction in this respect nicely supplements other charge exchange probes like the (p,n) reaction.[21]

For $J\neq 0$ targets, $E2$ contributions are allowed in $\Delta J=1$, $\Delta\pi=1$ transitions, increasing the number of matrix elements to be determined from the available experiments. The different experiments can be combined to give values for the individual matrix elements for comparison with theory, or to check certain assumptions, e.g., isospin invariance.

We show below that for the transition $^{13}C(\pi^-,\gamma)^{13}B$(g.s.), the observed branching ratio is almost completely due to the Gamow-Teller ($[\sigma\times Y_0]^1t^-$) matrix element, measured in ^{13}B beta decay. The contributions from other matrix elements are shown to be small. An upper limit on the spin-flip $E2$ matrix element ($[\sigma\times Y_2]^2$) is derived from the π-capture, beta decay, and electroexcitation data.

The relevant formulas connecting experimental data to many-body nuclear matrix elements are, in the notation of Ohtsubo and others[22] (see the Appendix):

For Gamow-Teller beta decay:

$$ft_{1/2}=318\frac{2J_i+1}{|\langle J_f||[\sigma\times Y_0]^1t^{\pm}||J_i\rangle|^2}\ . \tag{1}$$

For $M1$ electromagnetic decay:

$$\Gamma_0^{M1}=\frac{1}{2J_i+1}\left|\frac{\langle T_fT_f{}^310\,|\,T_iT_i{}^3\rangle_\gamma}{\langle T_fT_f{}^31+1\,|\,T_iT_i{}^3\rangle_\beta}\right|^2 E_{fi}{}^3\frac{8\pi}{3}\frac{e^2}{\hbar c}\frac{1}{4m_p{}^2c^4}|\langle J_f||([L\times Y_0]^1+4.71[\sigma\times Y_0]^1)t^-||J_i\rangle|^2\ . \tag{2}$$

Double-barred matrix elements are reduced with respect to angular momentum but not isospin. The units for $ft_{1/2}$, Γ_0, and E_{fi} are $\sec^{-1}$, eV, and MeV, respectively. We use $t^+|p\rangle=|n\rangle$ and note that the irreducible tensor operator t has components $(t^+,t^-,1/\sqrt{2}t_0)$. The notation $\langle T_fT_f{}^31m\,|\,T_iT_i{}^3\rangle_{\gamma,\beta}$ (Ref. 19) refers to the isospin Clebsch-Gordan coefficient appropriate for the electromagnetic or beta decay, respectively.

Simplifying Eq. (2) one obtains

$$\Gamma_0^{M1}=\frac{1}{2J_i+1}\left|\frac{\langle T_fT_f{}^310\,|\,T_iT_i{}^3\rangle_\gamma}{\langle T_fT_f{}^31\pm1\,|\,T_iT_i{}^3\rangle_\beta}\right|^2 E_{fi}{}^3\times 1.74\times10^{-2}\ \text{eV}\times|(L_{01}+4.71R_{01})|^2\ . \tag{3}$$

We introduce here the shorthand notations

$$R_{lJ}=\langle J_f||[\sigma\times Y_l]^Jt^-||J_i\rangle,\quad L_{lj}=\langle J_f||[L\times Y_l]^Jt^-||J_i\rangle\ ,$$

and

$$Y_l=\langle J_f||[Y_l]^Jt^-||J_i\rangle\ .$$

Similarly, the $E2$ decay width can be written:

$$\Gamma_0^{E2}=0.138\frac{1}{2J_i+1}\left|\frac{\langle T_fT_f{}^310\,|\,T_iT_i{}^3\rangle_\gamma}{\langle T_fT_f{}^31\pm1\,|\,T_iT_i{}^3\rangle_\beta}\right|^2 E_{fi}\,|\langle J_f||j_2(E_{fi}r/\hbar c)[Y_2]^2t^-||J_i\rangle|^2\ .$$

Simplifying this expression under the assumption that the radial wave function of all active nucleons is that of the $1p$ harmonic oscillator level, one obtains (with E_{fi} in MeV and r_0 in fm);

$$\Gamma_0^{E2}=2.54\times10^{-6}\ \text{eV}\frac{1}{2J_i+1}\left|\frac{\langle T_fT_f{}^310\,|\,T_iT_i{}^3\rangle_\gamma}{\langle T_fT_f{}^31\pm1\,|\,T_iT_i{}^3\rangle_\beta}\right|^2 E_{fi}{}^5r_0{}^4[Y_2]^2\ . \tag{4}$$

In these formulas isospin invariance is assumed, e.g., the only difference between the Gamow-Teller beta de-

cay matrix element $[\sigma\times Y_0]^1t^{\pm}$ and the spin part of the $M1$ amplitude $[\sigma\times Y_0]^1t^0$ is the isospin Clebsch-Gordan coefficients appearing in Eqs. (3) and (4).

For the radiative pion capture branching ratio one has the following expressions[9,22]:

$$R_\gamma=\sum_{l_\pi}\frac{f_{l_\pi}}{\Gamma_{l_\pi}}\frac{16\pi^2}{m_\pi c^2}\frac{E_\gamma}{(2J_i+1)(2l_\pi+1)}\times\frac{(1+m_\pi/m_N)^2}{(1+k/m_A)}$$
$$\times\sum_{J,L}\left\{|\langle J_f||M_a(J,L,l_\pi;r_n)||J_i\rangle|^2+|\langle J_f||M_b(J,L,l_\pi;r_n)||J_i\rangle|^2\right\} \quad (5)$$

with the operators given by Refs. 9 and 22. The operators M_a and M_b differ in parity and so may not give rise to interference terms. For $\Delta J=1^+$ transitions from 0^+ to 1^+ states, the following three operators contribute (notation is given in the Appendix):

$$M_a(1,1,0)=\frac{K_{1s}}{\sqrt{4\pi}}A\left[-\left[\tfrac{2}{3}\right]^{1/2}j_0[\sigma\times Y_0]^1t^+ +\frac{1}{\sqrt{3}}j_2[\sigma\times Y_2]^1t^+\right],$$

$$M_a(1,2,1)=\frac{K_{2p}}{\sqrt{4\pi}}\left\{(Arj_1+k(B+C)j_0)[\sigma\times Y_0]^1t^+-3\sqrt{2}\left[\frac{rA}{5}\left[j_3+\frac{j_1}{6}\right]+\frac{k}{3}\left[\frac{B}{2}-C\right]j_2\right][\sigma\times Y_2]^1t^+\right\},$$

$$M_b(1,1,1)=\frac{K_{2p}}{\sqrt{4\pi}}\left\{(-Arj_1+k(C-B)j_0)[\sigma\times Y_0]^1t^+ +\frac{1}{\sqrt{2}}(-Arj_1+k(B+2C)j_2)[\sigma\times Y_2]^1t^+\right\}.$$

For $\Delta J_\pi=1^+$ transitions from $\frac{1}{2}^-$ to $\frac{3}{2}^-$ states, four additional operators having rank $J=2$ contribute:

$$M_a(2,2,1)=\frac{K_{2p}}{\sqrt{4\pi}}\left\{(\sqrt{3}Dkj_2[Y_2]^2t^+)+\left[\frac{Ar}{5}(2j_3-3j_1)+Bj_2\right]\frac{1}{\sqrt{2}}[\sigma\times Y_2]^2t^+\right\},$$

$$M_b(2,1,1)=\frac{K_{2p}}{\sqrt{4\pi}}\left[\frac{3}{\sqrt{10}}(-Arj_1+kBj_2)[\sigma\times Y_2]^2t^+ +\left[\tfrac{3}{5}\right]^{1/2}kDj_2[Y_2]^2t^+\right],$$

$$M_b(2,2,0)=\frac{-K_{1s}}{\sqrt{4\pi}}(Aj_2[\sigma\times Y_2]^2t^+),$$

$$M_b(2,3,1)=\frac{K_{2p}}{\sqrt{4\pi}}\left[\left[\tfrac{8}{5}\right]^{1/2}(Arj_3+kBj_2)[\sigma\times Y_2]^2t^+-\left[\tfrac{12}{5}\right]^{1/2}kDj_2[Y_2]^2t^+\right]. \quad (6)$$

These expressions allow the beta decay ft value, $M1$ and $E2$ decay width, and (π^-,γ) branching ratio between analogous levels to be calculated in terms of matrix elements of just four operators. These are the following: R_{01}, the Gamow-Teller operator (analog of the spin part of $M1$); R_{21}, analog of the high momentum transfer spin-flip $M1$ operator; R_{22}, analog of the spin-flip $E2$ operator; and Y_2, analog of the charge-type $E2$ operator.

In the next section, Eq. (5) is evaluated for the ^{13}C$(\pi^-,\gamma)^{13}$B(g.s.) transition to show which matrix elements contribute most to the (π^-,γ) branching ratio, and to find out what new information can be gained.

B. The ^{13}C$(\pi^-,\gamma)^{13}$B(g.s.) transition

The reduction of Eq. (5) is made here, with the following assumptions: (a) the radial wave function of the active nucleons is that of a 1-p harmonic oscillator with $r_0=1.881\pm0.053$ fm (Ref. 23); (b) the pionic wave function distortion due to the strong interaction may be treated by the approximation method of distortion factors given in Ref. 1; (c) the (π,γ) interaction coefficients $A-D$ have the values and errors given as the "best fit" set in Ref. 1; (d) the 1s and 2p pionic widths and capture fractions are given by recent experimental results.[24]

The radiative capture branching ratio is then given as

$$R_\gamma=(5.38\pm0.74)\times10^{-3}\left\{(1.000\pm0.092)\,|R_{01}|^2-(0.033\pm0.016)\mathrm{Re}(R_{01}R_{21}^*)+(0.107\pm0.014)\,|R_{21}|^2\right.$$
$$\left.+(0.448\pm0.027)\,|R_{22}|^2+(0.014\pm0.004)\,|Y_2|^2-(0.097\pm0.015)\mathrm{Re}(Y_2R_{22}^*)\right\}. \quad (7)$$

This equation shows that the branching ratio is most sensitive to the Gamow-Teller matrix element $|R_{01}|$, somewhat less sensitive to the spin-flip $E2$ matrix element $|R_{22}|^2$, and practically insensitive to the other terms.

Inserting the value of $|R_{01}|^2=0.121\pm0.006$, found through Eq. (1) from the ^{13}B β decay ft value,[25] into Eq. (7), one predicts $R_\gamma=(6.51\pm1.12)\times10^{-4}$. This is in agreement with the present experimental result $R_0=(6.1\pm1.2)\times10^{-4}$.

The contribution of the $|Y_2|^2$ term can be computed using Eq. (4) and the (e,e') data on the analog ^{13}C(g.s.)$\rightarrow{}^{13}$C(15.11 MeV;$J^\pi,T=\frac{3}{2}^-,\frac{3}{2}$) transition.[26] One obtains $|Y_2|^2=0.14\pm0.03$, which gives a negligible contribution to R_γ in Eq. (7).

The value of $|R_{21}|^2$ cannot be extracted from the published ^{13}C(15.11 MeV;$J^\pi,T=\frac{3}{2}^-,\frac{3}{2}$) electroexcitation data because of the limited momentum-transfer range, and the difficulty of separating high momentum-transfer $M1$ from $E2$ contributions. However, the square of the single-particle matrix element for $p_{3/2}\rightarrow p_{1/2}$ via the R_{21} operator is only 0.053 (see the Appendix). Thus the contribution of R_{21} to R_γ in Eq. (7) may also be neglected.

An upper limit on the value of the spin-flip $E2$ matrix element $|R_{22}|^2$ can be obtained from Eq. (7) and the present experimental result. The one-standard-deviation limit is $|R_{22}|^2<0.05$. This is only about one-tenth of the single-particle value for $p_{3/2}\rightarrow p_{1/2}$. The spin-flip $E2$ strength in this transition thus appears to be strongly suppressed with respect to the Gamow-Teller strength, since $|R_{01}|^2$ amounts to 0.29 of its single-particle value in this transition.

The phenomenological analysis presented above shows that the Gamow-Teller matrix element measured in β decay accounts for essentially the full (π^-,γ) rate. The contribution of the many other possible terms of the mixed $M1/E2$ transition were thereby shown to be less than 10%.

Several other cases of strong isovector magnetic transitions in p-shell nuclei have been analyzed in this way. The (π^-,γ) rates are in all cases found to be accounted for by the lowest allowed multipolarity of $[\sigma\times Y_l]^J$ matrix elements. These results are summarized in Table III. The identity of (π^-,γ) strength with Gamow-Teller strength has been exploited in $A=20$ to separate the giant $M1$ transition there into spin and orbital parts, which was not otherwise possible due to the absence of the analog β decay transition.[11]

IV. DISCUSSION OF HIGH EXCITATION REGION

Prominent peaks above the breakup threshold have been observed in (π^-,γ) spectra throughout the $1p$ shell.[9] In the present work, peaks are seen at 6.5,

TABLE III. Comparison of spin-density matrix elements obtained from other experiments, to values inferred from (π^-,γ). Data for ^{6}Li, ^{12}C, ^{10}B from Ref. 9; ^{13}C from present work.

Operator	Multi-polarity	Transition	Other exp.	(π^-,γ)
$[\sigma\times Y_0]^1$	$M1$	^{6}Li(g.s.)$\rightarrow{}^6$He(g.s.)	0.617	0.627±0.034 (1s capture)
$[\sigma\times Y_0]^1$	$M1$	^{6}Li(g.s.)$\rightarrow{}^6$He(g.s.)	0.617	0.685±0.120 (2p capture)
$[\sigma\times Y_0]^1$	$M1$	^{12}C(g.s.)$\rightarrow{}^{12}$B(g.s.)	0.282±0.002	0.285±0.022
$[\sigma\times Y_0]^1$	$M1$	^{13}C(g.s.)$\rightarrow{}^{13}$B(g.s.)	0.348±0.009	0.335±0.010
$[\sigma\times Y_2]^3$	$M3$	^{10}B(g.s.)$\rightarrow{}^{10}$Be(g.s.)	0.70±0.06	0.64±0.04
$[\sigma\times Y_2]^3$	$M3$	^{10}B(g.s.)$\rightarrow{}^{10}$Be(3.37 MeV)	1.09±0.06	1.05±0.05

7.6, and 10.2 MeV excitation in ^{13}B (the analogs would occur at 21.6, 22.7, and 25.3 MeV excitation in ^{13}C). These peaks have been attributed to a $\Delta L=1$, $\Delta S=1$, $\Delta T=1$ spin-isospin giant dipole resonance of the target nuclide (^{13}C in the present work). The idea that a spin-isospin giant resonance component of $\Delta J^\pi=2^-$ character should exist near the $E1$ photoresonance energy[27,28] in fact motivated the earliest high resolution experiments with (π^-,γ).[1,4,8] Enough experiments and theoretical work now exist to show beyond reasonable doubt that the largest peaks seen in (π^-,γ) are due to this resonance. Furthermore, the observed strengths are of the order of full single-particle units. These spin-isospin excitations are $1\hbar\omega$ transitions involving spin flip, relative to the target ground state. They are associated with large spin-dipole matrix elements $[\sigma\times Y_1]^2$. The situation is similar to that of the $E1$ photoresonance, which in light nuclei still shows structure in the spectrum. The structure corresponds to the underlying $1\hbar\omega$ states strongly excited by photoabsorption, and does not form a smooth resonance peak as in heavier nuclei.

To demonstrate the existence, character, and strength of the spin-isospin states, three arguments are advanced below. First, the strength of the observed peaks in ^{13}B is compared with single particle estimates based on Eq. (5). Next, the $A=13$ spectrum is shown to agree with detailed shell model calculations in which the spin-dipole transitions induced by $[\sigma\times Y_1]^2$ dominate. Finally, the pattern of resonance splitting and energy shifts observed from $A=13$ to $A=20$ is discussed in terms of coupling of extra particles and holes to the underlying spin-dipole excitations of ^{12}C or ^{16}O cores.

A. Single particle estimates

A quantitative feeling for the strength of the peaks observed in the high excitation region can be gained by using Eq. (5) to compute the branching ratio expected for a single particle transition between pure configurations ($p_{3/2}$ to $d_{5/2}$ in this case, see Sec. III D) connected by the operator $[\sigma\times Y_1]^2t^+$. The strengths so obtained may be compared to single-particle strengths for the $E1$ photoresonance, found by comparing $E1$ widths from photoneutron data[29] to the Weisskopf unit values. The $\Delta J^\pi=2^-$ transition strengths in ^{13}C and ^{19}F are shown below to be of the order of a single-particle unit, and in fact 40% as strong as the $T=\frac{3}{2}$ part of the $T=\frac{3}{2}$, $E1$ photoresonance. This supports the interpretation of the (π,γ) spectrum in terms of excitation of relatively pure one-particle one-hole spin-dipole states (spin-isospin giant dipole resonance).

Transitions from $^{13}C_{g.s.}$ to $\frac{5}{2}^+$ states of ^{13}B may be excited by operators of multipolarities 2^- or 3^-. Four such operators contribute to radiative pion capture: $[\sigma\times Y_1]^2t^+$, $[\sigma\times Y_3]^2t^+$, $[Y_3]^3t^+$, and $[\sigma\times Y_3]^3t^+$. The first two are spin flip $M2$ and the last two are of $E3$ character. Vector coupling arguments show that $[\sigma\times Y_1]^2t^+$ should dominate for the transitions in question, if the final states are well described within the $1p$ and $2s$-$1d$ shells.[10] So let us consider only $[\sigma\times Y_1]^2t^+$ terms in Eq. (5) in computing single-particle estimates for the spin-dipole transitions.

The general form of $M_a(J,L,l_\pi)$ and $M_b(J,L,l_\pi)$ has been given by Ohtsuka[22]; we have reduced the expressions relevant to the case $J_i=\frac{1}{2}^-\rightarrow J_f=\frac{5}{2}^+$. These are given in the Appendix. Using these formulas in Eq. (5), the present data imply a matrix element

$$|\langle\tfrac{5}{2}^+,T=\tfrac{3}{2}||[\sigma\times Y_1]^2t^+||\tfrac{1}{2}^-,T=\tfrac{1}{2}\rangle|^2=0.40$$

to produce the sum of the three peaks's branching ratios. This may be compared with the value 0.67 obtained from Clebsch-Gordan algebra alone for a pure transition $p_{3/2}\rightarrow d_{5/2}$. The energy integrated transition strength is thus 0.6 times this "single particle" value. For the $E1$ photoresonance, the energy-integrated cross section to the $T=\frac{3}{2}$ giant dipole resonance (GDR) is about 100 mb MeV,[29] or only 1.5 W.u. One sees that the pion capture resonances have 40% as much strength in single-particle units, as does the $T=\frac{3}{2}$ photoresonance.

For the $^{13}C(\pi^-,\gamma)^{13}B$(g.s.) transition discussed earlier, Eq. (1) gives

$$|\langle J_f||[\sigma\times Y_0]^1t^+||J_i\rangle|^2=0.12$$

from the ^{13}B-beta decay ft value.[25] The single particle value for a pure $p_{3/2}\rightarrow p_{1/2}$ transition is 0.42, giving 0.29 single particle units for this transition. In Weisskopf units, the analogous $M1$ electroexcitation transition (^{13}C g.s.$\rightarrow^{13}$C 15.1 MeV) has 0.35 W.u., nearly exhausting Kurath's $M1$ sum rule.[30] Part of the difference comes from the contribution of

$$|\langle J_f||[L\times Y_0]^1t^+||J_i\rangle$$

to the $M1$ transition density.

The ^{19}F transitions to the doublet at 12.5 and 13.9 MeV in ^{19}F may also be compared to such a single particle estimate, although the large J values involved permit many contributions other than $[\sigma\times Y_1]^2$. The observed strength is 0.25 times that computed for a single particle $p_{1/2}\rightarrow d_{5/2}$ transition (see Sec. IV D for the choice of reference transition).

B. Comparison with shell model calculations

In Sec. II C, the similarity of the ^{12}C and ^{13}C spectra was discussed. The reasons for this similarity are clearly shown by the detailed shell model calculations available for both nuclei. From the ^{12}C case, where a full continuum shell model (CSM) calculation exists,[22] two facts relevant to the discussion of ^{13}C may be extracted. First, the contributions from the continuum to the prominent $\Delta J^\pi = 2^-$ resonance at 4.5 MeV in ^{12}B (19.6 MeV in ^{12}C) are small. Therefore the harmonic oscillator shell model (HOSM) calculations of the Dubna group[10,31] should be reliable, and in fact do agree well with the CSM for ^{12}C. Second, the dominant configuration of this state is $d_{5/2}p_{3/2}^{-1}$ mixing constructively with $s_{1/2}p_{3/2}^{-1}$. The first observation is important, since for ^{13}C only the HOSM calculations are available, and these reproduce the data rather well. The second observation provides the clue to the structure of the doublet of levels at 6.5 and 7.6 MeV in ^{13}B, which should have analogs at 21.6 and 22.7 MeV in ^{13}C. Coupling the extra neutron of ^{13}C weakly to the basic $\Delta J^\pi = 2^-$ core excitation produces a $\frac{3}{2}^+$ and $\frac{5}{2}^+$ doublet, in addition to a core polarization evidenced by an upward centroid shift of the doublet by 2.5 MeV. Both the splitting of the strength and the shift are predicted by the HOSM calculations and observed in our data.

The impulse-approximation calculations by Kissener and co-workers included initial and final state correlations generated by single-particle matrix elements similar to the Cohen-Kurath 2MBE set (for even parities) and a Gillet-type residual interaction (for odd parities). The full $0\hbar\omega$ and $1\hbar\omega$ basis was included.

Differing from the simplified treatment used above, the pionic atom wave functions used were explicitly evaluated by solving the Klein-Gordon equation numerically for a nuclear potential fitted to a

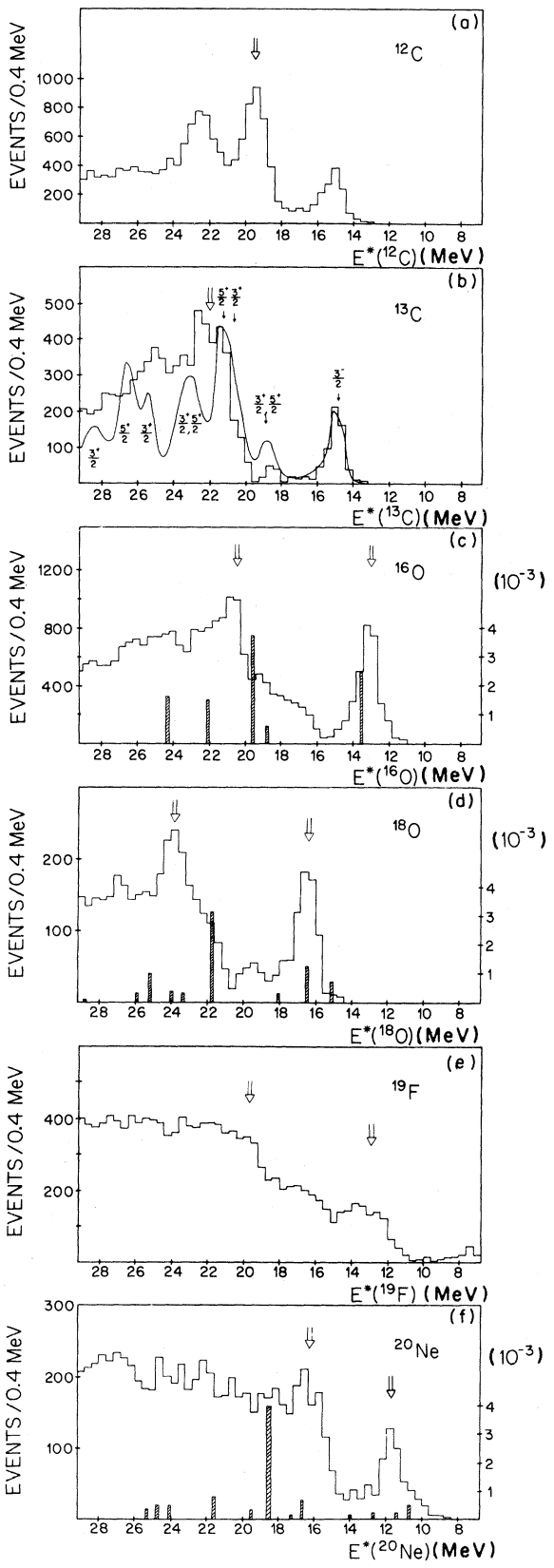

FIG. 5. Spin-quadrupole excitations in $A=12$ to 20. Displayed are the photon spectra from radiative pion capture in (a) ^{12}C (SIN) (Ref. 9), (b) ^{13}C, (c) ^{16}O (SIN) (Ref. 6), (d) ^{18}O (SIN) (Ref. 6), (e) ^{19}F, (f) ^{20}Ne (Ref. 11). The photon energy is converted into excitation energy relative to the target ground state. The arrow at higher excitation energies points to the $(p_{3/2}^{-1}d_{5/2})$ $J^\pi=2^-$ configuration or the corresponding multiplet of states (^{19}F, ^{13}C). The arrow at lower energies points to the equivalent $(p_{1/2}^{-1}d_{5/2})$ structure. The solid curve drawn into the ^{13}C spectrum represents the calculations of Kissener *et al.* (Ref. 10) with the yield normalized to the ^{13}B ground state (15.1 MeV). The vertical bars (right scale) show the results for the photon yield per pion stopped as calculated by Knüpfer (Ref. 37) (^{16}O, ^{18}O, and ^{20}Ne).

large body of pionic atom data. The 1s and 2p capture probabilities used were 8% and 92%, respectively. The pionic total widths of the 1s and 2p states were taken to be the same as for ^{12}C, 2.96 keV and 1.02 eV, respectively. These values do not differ significantly from the experimental values found for ^{13}C, $\Gamma_{1s}=2.45\pm0.10$ keV and $\Gamma_{2p}=0.97\pm0.10$ eV, which have recently become available.[24]

In Fig. 5, the calculated curve from Ref. 10 is superimposed on the measured ^{13}C spectrum. With the theoretical strength normalized to fit the ^{13}B ground state data, reasonable agreement in relative strengths and peak positions is obtained. Since the prediction for ^{13}C$(\pi^-,\gamma)^{13}$B(g.s.) is 12.8×10^{-4} while the observed branching ratio is only $(6.1\pm1.2)\times10^{-4}$, all theoretical rates exceed the experimental ones by at least a factor of 2 (see Table I).

The predicted spectrum falls below the data at lower photon energies. This is to be expected since the HOSM calculation considered only final states reached by $0\hbar\omega$ and $1\hbar\omega$ transitions. In the case of ^{16}O, the contribution of $2\hbar\omega$ and higher configurations has been shown to fill up this part of the spectrum with a smooth shape, due to the enormous number of states involved.[31,32] Direct processes will contribute here as well.

The calculated transitions are mainly driven by the $[\sigma\times Y_1]^2$ part of the (π^-,γ) transition operator, leading to $J^\pi=\frac{3}{2}^+,\frac{5}{2}^+$ for the excited states. This piece of the operator is also responsible for the strong 2^- transitions in ^{12}C(π^-,γ), as well as the preferred excitation of analogs of $M2$ states throughout the 1p shell.[6,10]

The (π^-,γ) branching ratios are quite sensitive to the configuration mixing. For example, the first predicted doublet results from the destructive interference of the two configurations mentioned above $(d_{5/2}p_{3/2}{}^{-1}$ and $s_{1/2}p_{3/2}{}^{-1})$. These same configurations are predicted to interfere constructively in forming the upper doublet, which is predicted to be much stronger than observed in the experiment.

Unfortunately, the capture of π^- at rest occurs at fixed momentum transfer. Therefore the real experimental proof of the spin and parity of these states must come from other reactions. Electron scattering data are limited,[33] but show a rise in the backward cross section near 22.5 MeV in ^{13}C, which could be ascribed to $M2$ transition strength. Other charge exchange probes like (p,n) have recently added support to our assignments.[21]

C. Spin-quadrupole strength from $A=13$ to 20

Figure 5, which shows the radiative pion capture spectra from $A=13$ to 20 (not including $A=14$), will serve as the basis for a qualitative discussion of the distribution of $\Delta J^\pi=2^-$ strength near ^{16}O. The data on the oxygen isotopes are from Ref. 6; the ^{20}Ne data were taken by us during the same period as the ^{13}C and ^{19}F data.[11]

In ^{16}O, four of the five possible one-particle one-hole combinations[34] which can form a $\Delta J^\pi=2^-$ ($M2$) transition carry all the isovector spin-quadrupole strength.[31,32,35] The configurations and approximate excitation energies relative to the ^{16}O ground state are given in Table IV. The residual interaction mixes only the third and the fourth, because they are most nearly degenerate. Otherwise the configurations of the observed states remain rather pure, although 3-p 3-h admixtures do occur. The observed (π^-,γ) spectrum shows the 2_1^- (^{16}N g.s.) and 2^{4-} (^{16}N 7.4 MeV) levels. The latter has the configuration[35]

$$|2_4^-\rangle=0.60\,|2s_{1/2}1p_{3/2}^{-1}\rangle+0.75\,|1d_{5/2}1p_{3/2}{}^{-1}\rangle\ .$$

Especially the configurations with a $d_{5/2}$ particle are connected to the ground state by large single-particle $M2$ matrix elements. The 2_3^- configuration is nearly orthogonal to the $2_4{}^{-1}$ state[31,35]:

$$|2_3^-\rangle=0.79\,|2s_{1/2}1p_{3/2}{}^{-1}\rangle-0.54\,|1d_{5/2}1p_{3/2}{}^{-1}\rangle\ .$$

The minus sign between the contributions results in cancellations, reducing the calculated transition strength. Nevertheless, all four 2^- states are experimentally observed,[9] and the relative strengths are correctly predicted.

Qualitatively, the observed distribution of transition strength in ^{12,13}C, ^{16}O, ^{18}O, ^{19}F, and ^{20}Ne is consistent with weak coupling of extra particles to $\Delta J^\pi=2^-$ excitations of a ^{16}O core. Starting with the oxygen isotopes, two added neutrons in ^{18}O hardly change the spectrum shape. The response is merely shifted upwards by amounts ranging from 2.8 MeV (2_4^-) to 3.2 MeV (2_1^-). This agrees with the core polarization model calculations by Knupfer and Huber[7,36] in which the neutrons are weakly coupled to 2^- states of the ^{16}O core.

In ^{12}C only $p_{3/2}$ hole states can be formed; the dominant peak is expected to be mainly

TABLE IV. The five $J^\pi,T=2^-,1$ one-particle, one-hole states in ^{16}O.

State	Dominant configuration	Excitation energy in ^{16}O
2_1^-	$1d_{5/2}1p_{1/2}{}^{-1}$	13 MeV
2_2^-	(not seen)	
2_4^-	$2s_{1/2}1p_{3/2}{}^{-1}$	19
2_4^-	$1d_{5/2}1p_{3/2}{}^{-1}$	20
2_5^-	$1d_{3/2}1p_{3/2}{}^{-1}$	23

$1d_{5/2}1p_{3/2}{}^{-1}$. It is observed at nearly the same energy relative to ^{12}C (g.s.) as it was in ^{16}O (19.5 vs 20.4 MeV), showing little effect due to the additional quartet of $p_{1/2}$ nucleons in ^{16}O. The addition of an unpaired neutron to ^{12}C (forming ^{13}C) again shifts the whole response upward (by 2.5 MeV), and splits the main peak into a narrow doublet.

Adding a quartet of nucleons to ^{16}O (forming ^{20}Ne) also leaves the dominant core excitations unchanged but shifts the response to *lower* energies by about 4 MeV. We identify the main peaks in the ^{20}Ne spectrum at (11.6, 12.1) MeV and near 16.4 MeV, with the structures at 13 and 20 MeV in ^{16}O, respectively. For the lower structure in ^{20}Ne the level assignment is known; the upper one is made on the basis of predictions.[36] However, the detailed configurations have not been published.

From the systematics of these shifts, the corresponding states in ^{19}F should lie around 12 to 13 MeV and 20 MeV, and should further be split into several levels ($J=\frac{1}{2}$ to $\frac{7}{2}$ are possible). This is indeed the case, if the two ^{19}O levels at 4.9 and 6.3 MeV (12.5 and 13.9 MeV in ^{19}F) are tentatively associated with the 2_1^- state, and the sharp step in transition strength near 12 MeV (20 MeV in ^{19}F) is associated with overlapping levels built on the 2_4^- structure in ^{16}O. The spin-parity assignments for known levels of ^{19}O in this region of excitation ($\frac{3}{2}^-$, $\frac{1}{2}^-$ at 4.6 and 5.1 MeV; $\frac{7}{2}^-$ and $\frac{1}{2}^-$ at 6.3 and 6.2 MeV) lend support to these interpretations.

Table V summarizes the experimental branching ratios and the results of several calculations for the (π^-,γ) transitions leading to $M2$ states built on 2_4^- ($d_{5/2}p_{3/2}{}^{-1}$) and 2_1^- ($d_{5/2}p_{1/2}{}^{-1}$). Experimentally, the 2_4^- configuration remains pure, carrying about the same strength for all the nuclides. The 2_1^- configuration becomes weaker as nucleons are added to ^{16}O. The calculations of Knupfer[37] for ^{16,18}O and ^{20}Ne, and of Kissener *et al.*[10] for the carbon isotopes reproduce the observed pattern. The calculated branching ratios are always about a factor of 2 larger than experiment. Most of the quenching is due to two-particle two-hole admixtures in the "closed shell" ground state of ^{16}O. Including these admixtures in the calculations[31,32] reduces the predicted branching ratios by a factor of 0.6 for ^{16}O.[38]

Speth *et al.*[39] recently connected the missing experimental strength for $BM2$ values of the large 2^- states in ^{16}O to the presence of ρ meson exchange in the effective nucleon-nucleon potential. Although we cannot quantitatively compare with the present data, the same spin density matrix elements are involved here, with a similar reduction of experimental transition strength with respect to theory.

The selectivity of the reaction, as demonstrated in considerable existing data, show that the present (π^-,γ) results may be used as a guide to the location of strong spin-flip excitations in, for example, electron-scattering or (p,n) experiments. Such a procedure has proven useful already for ^{18}O.[40]

The behavior of the spin-isospin dipole resonance may be compared with that of the $E1$ photoresonance (isospin mode). The main features of the $E1$ photoresonance in a shell model picture are accounted for by the schematic model of Brown and Bosterli.[41] If only the single particle shell model potential is considered, a number of transitions of a given multipolarity may be available to valence nucleons. If these transitions are degenerate in energy or nearly so, even a weak residual interaction among the nucleons may profoundly change the distribution of transition strength by strongly mixing the single particle states involved.

Especially in light nuclei, the degeneracy of the $\Delta L=1$, $\Delta S=0$ single particle states may be broken by pairing forces, deviation from spherical symmetry as in distorted nuclei, etc. In these cases the

TABLE V. Summary of major $M2$ strengths observed and calculated, for (π^-,γ) transitions near the ^{16}O shell.

Configuration		$R_\gamma\times10^{-4}$ ^{12}C	^{13}C	^{16}O	^{18}O	^{19}F	^{20}Ne
	exp.	18.3±0.6[a]	18.8±2.8	15.1±1.6[b]	18.1±2.2[b]		15.3±2.0
$d_{5/2}p_{3/2}{}^{-1}$	theory		34[c]	37[d]	37[d]		40[d]
	ratio		0.55	0.41	0.49		0.38
	exp.			14.5±1.6[b]	12.3±1.6[b]	9.3±1.5	4.3±1.7
$d_{5/2}p_{1/2}{}^{-1}$	theory			25[d]	20[d]		11[d]
	ratio			0.58	0.61		0.40

[a]Reference 9.
[b]Reference 6.
[c]Reference 10.
[d]Reference 37.

photoresonance may appear broadened, split, or disrupted entirely. This behavior is nicely shown in the photoneutron data of Veysiere,[42] comparing, for example, ^{16,18}O and ^{19}F.

In the case of $M2$-type transitions, the single particle states are split into two groups by the spin-orbit coupling. Though in odd A nuclei like ^{19}F the single particle spectrum can be so spread out that no distinct resonance is formed, the strong spin-orbit splitting leaves the two broadened components of the isovector $M2$ strength still visible, in many cases (e.g., ^{16}O).

IV. SUMMARY

The (π^-,γ) energy spectra and branching ratios for ^{13}C(π^-,γ) and ^{19}F(π^-,γ) have been measured. A detailed comparison of ^{13}C$(\pi^-,\gamma)^{13}$B(g.s.), ^{13}B β decay, and ^{13}C$(e,e')^{13}$C(15.11 MeV, $J^\pi=\frac{3}{2}^-$ $T=\frac{3}{2}$) shows that the Gamow-Teller operator accounts for essentially the full (π^-,γ) rate.

(π^-,γ) transitions leading to excited states of ^{13}B at 6.5, 7.6, and 10.2 MeV (analogs at 21.6, 22.7, and 25.3 MeV in ^{13}C) have been compared to the ^{13}C(γ,n) cross section. It has been shown that the strength of the (π^-,γ) resonances, measured in appropriate single particle units, is 0.6 units in the squared amplitude, while that of the $T=\frac{3}{2}$ part of the $E1$ photoresonance is about 1.5 W.u. This large strength is evidence for the identification of the (π^-,γ) resonances as analogs of the spin isospin component of the ^{13}C giant dipole resonance. This interpretation is supported by shell model calculations, which point to the preferred excitation of analogs of $M2$ states of the target nuclide. The excitations are driven primarily by the operator $[\sigma\times Y_1]^2$, with the $d_{5/2}p_{3/2}{}^{-1}$ configuration being a prominent feature of (π^-,γ) spectra from $A=13$ to 20. Coupling of extra nucleons to this underlying core excitation tends to shift and split levels, but leaves unchanged the summed branching ratio. This is not the case for the other major structure based on $d_{5/2}p_{1/2}{}^{-1}$, which becomes weaker and increasingly fragmented, with more nucleons in the $2s$-$1d$ shell.

ACKNOWLEDGMENTS

The experiments upon which this work is based could not have been completed without the contributions of the Lawrence Berkeley Laboratory Nuclear Instrumentation Group under S. R. Olsen, who designed and built the multiwire chamber electronics; J. M. Gallup, E. Lieberman, and S. Schlaer, who provided essential software support; and the staff of LAMPF, who provided cryogenic support for the liquid hydrogen target. We sincerely thank these people. The work was done under the sponsorship of the Office of Energy Research, U.S. Department of Energy, under Contract No. DE-AC073-76SF00098, and that of the Swiss National Science Foundation.

APPENDIX

We use $\hbar=c=1$ except in expressions containing $e^2/\hbar c=\frac{1}{137}$. Certain notations used in Eqs. (1)–(4) are defined below.

(1) The operator product of two irreducible tensor operators T (rank k) and Q (rank l) is

$$[T_k\times Q_l]^{Jm}=\sum_{m_k,m_l}\langle km_k,lm_l\,|\,Jm\rangle T_{km_k}Q_{lm_l}\,.$$

The first quantity in the summation is a Clebsch-Gordan coefficient.

(2) The isospin Clebsch-Gordan coefficients

$$\langle T_fT_f{}^31m\,|\,T_iT_i{}^3\rangle_\gamma$$

or β connect initial and final states in radiative $(m=0)$ or β_+^- $(m=\pm1)$ decays. These must appear explicitly if it is desired to always use the charge changing matrix elements R_{lj} and L_{lj}.

(3) The matrix elements R_{lJ} and L_{lJ} are many-body matrix elements between the initial and final nuclear states. In the impulse approximation, these are each a sum over all particles in the nucleus of the single particle operators given in their definitions.

(4) E_{fi} is the excitation energy of a state (usually observed in electroexcitation).

(5) j_l is the spherical Bessel function of order l and argument qr, with q the momentum transfer in the reaction and r the radial coordinate of nucleons.

(6) m_p is the proton mass, m_π is the pion mass, m_A is the nuclear mass, and k is the photon momentum.

(7) Subscripts zero as in Γ_0^{M1} indicate that extrapolation to $q=E_{fi}$ has been performed in the analysis of electroexcitation data.

(8) Radial matrix elements have been evaluated assuming $1p$ and/or $1d$ harmonic oscillator wave functions

$$(\alpha\, r^l\exp(-r^2/2r_0{}^2))\,,$$

with r_0 taken from electron scattering. For ^{13}C, $r_0=1.881\pm0.053$ has been used (Ref. 23).

(9) $f_{l\pi}$ from Eq. (5) is the fraction of all pion captures occurring from the pionic orbital with quantum numbers symbolized by l_π. The total width of such an orbital 1*s* is denoted by $\Gamma_{l\pi}$.

(10) In the equations after Eq. (5), the coefficients A,B,C,D are part of the $(\pi\gamma)$ interaction Hamiltonian. The numerical values used have been those of the "recommended" set from Ref. 1, with uncertainties.

(11) The coefficients K_{nl} appearing in the pion capture transition operators come from the pionic atom wave functions of the initial states:

$$K_{1s}=2\sqrt{C_{1s}}a_\pi^{-3/2}\ ,$$

$$K_{2p}=\frac{1}{2\sqrt{6}}\sqrt{C_{2p}}a_\pi^{-5/2}\ .$$

The distortion factors C_{nl} are discussed in Ref. 1, and the values used here for ^{13}C and ^{19}F, respectively, were those for ^{12}C and ^{16}O, given in Table V of that work. The symbol a_π is the Bohr radius of the ground state pionic atom.

(12) The formula which we have used for evaluating single particle matrix elements of spin-multipole operators is given by Ohtsuka[22] (p. 66)

$$\langle l'j'||[\sigma\times Y_L]^J||lj\rangle=(-)^{1+L-J}\tfrac{1}{2}[1+(-)^{l'+l+L}]\left[\frac{j(j+1)}{4\pi}\right]^{1/2}$$

$$\times\begin{cases}(-)^{j+J+j'}\sqrt{J}\,(j\,1/2J0\,|\,j'1/2)-(-)^{l'+1/2-j'}\sqrt{J+1}(j-1/2J1\,|\,j'1/2) & \text{for } J=L+1\ ,\\ (-)^{l'+1/2-j'}(2J+1)^{1/2}(j-1/2J1\,|\,j'1/2) & \text{for } J=L\ ,\\ (-)^{j+J-j'}\sqrt{J+1}(j\,1/2J0\,|\,j'1/2)-(-)^{l'+1/2-j'}\sqrt{J}\,(j-1/2J1\,|\,j'1/2) & \text{for } J=L-1\ .\end{cases}$$

The operators for $\Delta J^\pi=2^-$ transitions from $\frac{1}{2}^-\rightarrow\frac{5}{2}^+$ are the following for the 2*p* pion capture

$$M_a(2,1,1)=\frac{K_{2p}}{\sqrt{4\pi}}\left[\tfrac{2}{3}\right]^{1/2}\left\{\left[-Ar\left[j_0+\frac{j_2}{10}\right]+\tfrac{9}{10}kj_1\left[B-\tfrac{2}{3}C\right]\right]t^+[\sigma\times Y_1]^2\right.$$
$$\left.+\tfrac{3}{5}[Arj_2-kj_3(B+C)]t^+[\sigma\times Y_3]^2\right\},$$

$$M_a(2,3,1)=\frac{K_{2p}}{\sqrt{4\pi}}\left\{\frac{2\sqrt{6}}{5}(Arj_2+j_1k(B+C))t^+[\sigma\times Y_1]^2\right.$$
$$\left.+\tfrac{1}{7}[-6Ar(j_4+\tfrac{1}{15}j_2)+\tfrac{42}{5}(C-\tfrac{2}{3}B)kj_3]t^+[\sigma\times Y_3]^2\right\},$$

$$M_a(3,3,1)=\frac{K_{2p}}{\sqrt{4\pi}}\{[\tfrac{2}{7}Ar(\tfrac{3}{4}j_4-j_2)+\tfrac{1}{2}Bkj_3]t^+[\sigma\times Y_3]^3+\sqrt{3}Dkj_3t^+[Y_3]^3\}\ ,$$

$$M_b(2,2,1)=\frac{K_{2p}}{\sqrt{4\pi}}\left\{\left[\frac{3}{2\cdot5}\right]^{1/2}(-Arj_2+kj_1(2C-B))t^+[\sigma\times Y_1]^2\right.$$
$$\left.+\frac{1}{\sqrt{5}}\left[-Arj_2+3kj_3\left[\frac{B}{3}+C\right]\right]t^+[\sigma\times Y_3]^2\right\},$$

$$M_b(3,2,1)=\frac{K_{2p}}{\sqrt{4\pi}}\left\{\frac{2\sqrt{2}}{\sqrt{7}}(-Arj_2+kj_3B)t^+[\sigma\times Y_3]^3+\frac{\sqrt{3}}{2}Dkt^+[Y_3]^3\right\},$$

$$M_b(3,4,1)=\frac{K_{2p}}{\sqrt{4\pi}}(\tfrac{5}{7})^{1/2}\{\tfrac{3}{2}(Arj_4+Bkj_3)t^+[\sigma\times Y_3]^3-\sqrt{3}Dj_3t^+[Y_3]^3\}\ ,$$

and for the 1*s* capture

$$M_a(2,2,0)=\frac{K_{1s}}{\sqrt{4\pi}}\{-(\tfrac{3}{5})^{1/2}Aj_1t^+[\sigma\times Y_1]^2+(\tfrac{2}{5})^{1/2}Aj_3t^+[\sigma\times Y_3]^2\}\ .$$

In the above expressions, the arguments of the Bessel functions are always kr.

*Present address: Department of Physics, Stanford University, Stanford, CA 94305.
†Permanent address: Institute of Nuclear Science, Tokyo, Japan.
‡Present address: Physics Department, Boston University, Boston MA 02215.
§Permanent address: National Instituut Kernphysik Sec. K, Amsterdam, The Netherlands.
**Present address: Finkenweg 45, D-8011 Oberpframmern, Federal Republic of Germany.

[1]H. W. Baer, K. M. Crowe, and P. Truoel, Adv. Nucl. Phys. 9, 177 (1977) (review).
[2]J. P. Perroud, in *Photopion Nuclear Physics,* edited by P. Stoler (Plenum, New York, 1978), p. 69 (review).
[3]P. Truoel, *Lecture Notes in Physics* (Springer, New York, 1979), Vol. 108, p. 351 (review).
[4]J. A. Bistirlich, K. M. Crowe, A. S. L. Parsons, P. Skarek, and P. Truoel, Phys. Rev. Lett. 25, 689 (1970).
[5]J. A. Bistirlich, K. M. Crowe, A. S. L. Parsons, P. Skarek, and P. Truoel, Phys. Rev. C 5, 1867 (1972).
[6]G. Strassner, P. Truoel, J. C. Alder, B. Gabioud, C. Joseph, J. F. Loude, N. Morel, A. Perrenoud, J. P. Perroud, M. T. Tran, E. Winkelmann, W. Dahme, H. Panke, D. Renker, and H. A. Medicus, Phys. Rev. C 20, 248 (1979).
[7]W. Knupfer and M. G. Huber, Proceedings of the International Conference on Nuclear Reaction Mechanism, Varenna, 1977, p. 343.
[8]H. W. Baer, J. A. Bistirlich, N. deBotton, S. Cooper, K. M. Crowe, P. Truoel, and J. D. Vergados, Phys. Rev. C 12, 921 (1975).
[9]A. Perroud *et al.*, University of Lausanne, report 1981; A. Perrenoud, thesis, University of Lausanne, 1979.
[10]H. R. Kissener, G. E. Dogotar, R. A. Eramzhyan, and R. A. Sakaev, Nucl. Phys. A312, 394 (1978); Dubna Report 11275, 1978.
[11]C. J. Martoff, J. A. Bistirlich, K. M. Crowe, M. Koike, J. P. Miller, S. S. Rosenblum, W. A. Zajc, A. H. Wapstra, G. Strassner, and P. Truoel, Phys. Rev. Lett. 46, 891 (1981).
[12]S. R. Olsen, F. A. Kirsten, E. P. Binnall, K. L. Lee, N. N. Bhandari, and C. C. Nunnally, Lawrence Berkeley Laboratory Report No. LBL-2245, 1973.
[13]J. Spuller, D. Berghofer, M. D. Hasinoff, R. MacDonald, M. Measday, T. Salomon, T. Suzuki, J. M. Poutissou, R. Poutissou, and J. K. P. Lee, Phys. Lett. 67B, 479 (1977).
[14]We thank R. Macek of LAMPF for the loan of this target.
[15]C. J. Martoff, thesis, University of California, Berkeley, Lawrence Berkeley Laboratory Report LBL-10954, 1980.
[16]H. von Fellenberg, thesis, University of Zurich, 1978.
[17]J. C. Alder, B. Gabioud, C. Joseph, J. F. Loude, N. Morel, A. Perrenoud, M. T. Tran, B. Vaucher, E. Winkelman, D. Renker, H. Schmidt, Č. Zupančič, H. von Fellenberg, A. Frischknecht, F. Hoop, G. Strassner, and P. Truoel, Nucl. Instrum. Methods 160, 93 (1979).
[18]L. Dakhno and Y. Prokoshkin, Yad. Fiz. 7, 565 (1968) [Sov. J. Nucl. Phys. 7, 351 (1968)].
[19]F. S. Dietrich, M. Suffert, A. V. Nero, and S. S. Hanna, Phys. Rev. 168, 1169 (1968).
[20]S. S. Hanna, in *Isospin in Nuclear Physics,* edited by D. H. Wilkenson (North-Holland, Amsterdam, 1969), p. 602.
[21]C. D. Goodman, Comments Nucl. Part Phys. 10, 117 (1981), and references therein.
[22]N. Ohtusubo, T. Nishiyama, and M. Kawaguchi, Nucl. Phys. A224, 164 (1974); N. Ohtsuka, thesis, Osaka University, 1978.
[23]B. T. Chertok, C. Sheffield, J. W. Lightbody, S. Penner, and D. Blum, Phys. Rev. C 8, 23 (1973).
[24]C. A. Fry, J. G. A. Beer, G. R. Mason, R. M. Pearce, R. R. Poffenberger, C. I. Sayre, A. Olin, and J. A. Macdonald, Nucl. Phys. A375, 325 (1982).
[25]K. W. Jones, W. R. Harris, M. T. Ellistrem, and D. E. Alburger, Phys. Rev. 186, 978 (1969).
[26]G. Wittwer, H.-G. Clerc, and G. A. Beer, Phys. Lett. 30B, 634 (1969).
[27]J. D. Walecka, in *Preludes in Theoretical Physics,* edited by A. de Shalit (Wiley, New York, 1966), p. 59.
[28]H. Ueberall, in *High Energy Physics and Nuclear Structure,* edited by S. Devons (Plenum, New York, 1970), p. 48.
[29]J. W. Jury, B. L. Berman, D. D. Fall, P. Meyer, K. G. McNeill, and J. G. Woodworth, Phys. Rev. C 19, 1684 (1979).
[30]D. Kurath, Phys. Rev. 130, 1525 (1963).
[31]R. A. Eramzhyann, M. Gmitro, and H. R. Kissener, Nucl. Phys. A290, 294 (1977); A338, 436 (1980).
[32]J. D. Vergados, Phys. Rev. C 12, 127 (1975).
[33]J. C. Bergstrom, H. Crannel, F. J. Kline, J. T. O'Brien, J. W. Lightbody, and S. P. Fivozinsky, Phys. Rev. C 4, 1514 (1971).
[34]J. Meyer-ter Vehn, Phys. Rep. 74, 324 (1981).
[35]M. Gmitro, S. S. Kamalov, T. V. Moskaulenko, and R. A. Eramzhyan, Czech. J. Phys. B31, 495 (1981).
[36]W. Knüpfer, H. Ender, and M. G. Huber, in *Proceedings of the Eighth International Conference on High Energy Physics and Nuclear Structure, Vancouver, 1979,* edited by D. F. Measday and A. W. Thomas (North-Holland, Amsterdam, 1980).
[37]W. Knüpfer, private communication; see also Ref. 36.
[38]We feel that the uncertainties from the pionic atom capture schedules and the $2p$ widths are on the average eliminated when several nuclides are considered.
[39]J. Speth, V. Klemt, J. Wambach, and G. E. Brown, Nucl. Phys. A343, 282 (1980).
[40]E. J. Ansaldo, C. Ranzacharyulu, D. Bender, U. Kramer, A. Richter, E. Spaner, and W. Knüpfer, Phys. Lett. 95B, 31 (1980).
[41]G. E. Brown and M. Bosterli, Phys. Rev. Lett. 3, 472 (1959).
[42]A. Veysière, K. G. McNeill, J. W. Jury, R. A. Alvarez, B. L. Berman, D. D. Fall, and P. Meyer, Phys. Rev. C 19, 1667 (1979).